

Toward Practical Self-Supervised Monocular Indoor Depth Estimation

Cho-Ying Wu^{1,2*}, Jiali Wang¹, Michael Hall¹, Ulrich Neumann² and Shuochen Su¹

¹Meta Reality Labs, ²University of Southern California

{jialiaw, michaelhall, shuochsu}@fb.com, {choyingw, uneumann}@usc.edu

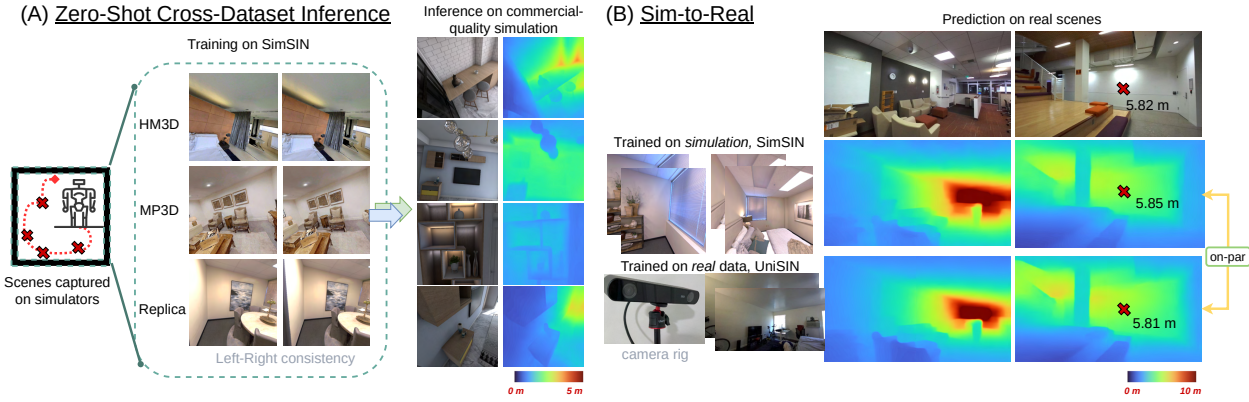


Figure 1. **Advantages of our framework.** (A) We attain zero-shot cross-dataset inference. (B) Our framework trained on simulation data produces on-par results with the one trained on real data.

Abstract

The majority of self-supervised monocular depth estimation methods focus on driving scenarios. We show that such methods generalize poorly to unseen complex indoor scenes, where objects are cluttered and arbitrarily arranged in the near field. To obtain more robustness, we propose a structure distillation approach to learn knacks from a pre-trained depth estimator that produces structured but metric-agnostic depth due to its in-the-wild mixed-dataset training. By combining distillation with the self-supervised branch that learns metrics from left-right consistency, we attain structured and metric depth for generic indoor scenes and make inferences in real-time. To facilitate learning and evaluation, we collect SimSIN, a dataset from simulation with thousands of environments, and UniSIN, a dataset that contains about 500 real scan sequences of generic indoor environments. We experiment in both sim-to-real and real-to-real settings, and show improvements both qualitatively and quantitatively, as well as in downstream applications using our depth maps. This work provides a full study, covering methods, data, and applications. We believe the work

lays a solid basis for practical indoor depth estimation via self-supervision.

1. Introduction

This work proposes a **practical** indoor depth estimation framework that has the following features: *learning without curated depth annotations*, *efficient training data collection*, *high generalizability to cross-dataset inference*, and *accurate and real-time depth sensing*.

Although self-supervised depth estimation has attracted much research interest recently, popular works, such as MonoDepth [24], MonoDepth2 [25], DepthHints [75], and ManyDepth [76], mainly focus on driving scenes and are trained on large-scale driving datasets like KITTI [23] and Cityscapes [14]. Self-supervised learning of *indoor* depth is arguably more challenging for a number of reasons: (1) *structure priors*: depth estimation for driving scenes imposes a strong scene structure prior to the learning paradigm. The upper parts of images, commonly occupied by the sky or buildings, are typically farther away; on the other hand, the lower parts are usually roads extending to the distance [16]. By contrast, the structure priors are much

*Work done while interning at Meta Reality Labs.

weaker for indoor environments since objects can be cluttered and arranged arbitrarily in the near field. (2) *distribution*: scene depth for driving scenarios tends to distribute more evenly across near to far ranges on roads, whereas indoor depth can be concentrated in either near or far ranges, such as close views of desks or ceilings. The uneven depth distribution makes it challenging to predict accurate metric depth for indoor scenes. (3) *camera pose*: depth-sensing devices can move in 6DoF for indoor captures, but they are typically anchored on cars for collecting driving data where translations are usually without elevation and rotations are dominated by yaw angle. Therefore, a desirable network needs to be more robust to arbitrary camera poses and complex scene structures for indoor cases. (4) *untextured surfaces*: large untextured regions, such as walls, make the commonly used photometric loss ambiguous.

In this work, we propose *DistDepth*, a method to distill depth-domain structure knowledge from a transformer-based network, DPT [58, 59], that produces *structured but only relative* depth (output values reflect relative relations but are metric-agnostic). Our distillation strategy encourages depth structural similarity statistically as well as spatial occluding boundary similarity such that structural information can be blended into the self-supervised depth estimator effectively. In this way, given a single image at test time, our depth estimator can predict highly structured and metric-accurate depth for general indoor scenes (Sec. 3.2). Distillation also helps downsize the large vision transformer to a smaller architecture, which enables real-time depth estimation on portable devices.

We next describe our dataset-level contributions. Current publicly available stereo datasets are either targeting driving scenarios [9, 14, 21, 23, 77], small-scale and lacking scene variability [63, 64], rendered from unrealistic-scale 3D animations [6, 51], or collected in-the-wild [32, 70]. Popular indoor datasets are either small-scale (Middlebury [63]) or lacking stereo pairs (NYUv2 [53]). There is currently no large-scale indoor stereo dataset to facilitate left-right consistency for self-supervision. We thus utilize the popular Habitat simulator [61, 69] from embodied AI research to collect stereo pairs in 3D indoor environments. Commonly-used environments are chosen, including Replica [68], Matterport3D (MP3D) [8], and Habitat-Matterport 3D (HM3D) [56], to create *SimSIN*, a novel dataset consisting of about 515K Simulated stereo indoor images across about 1K indoor environments (Sec. 4). With SimSIN, we are able to investigate performances of prior self-supervised depth estimation frameworks on indoor scenes [25, 75, 76]. We show that we can fit on SimSIN by directly training those models, but such models generalize poorly to heterogeneous domain of unseen environments. Using our structure distillation strategy, however, can produce highly structured and metric-accurate depth on unseen data (Sec. 5).

Several commercial-quality simulations and real data are utilized for evaluation, including a challenging virtual apartment (VA) sequence [1, 2], pre-rendered scenes in Hypersim [60], and real monocular images in NYUv2 [67]. To further investigate the gap between training on simulation v.s. training on real data, we further collect *UniSIN*, a dataset including 500 real stereo indoor sequences and about 200K images in a university across buildings and multi-purpose spaces using off-the-shelf high-performing stereo cameras. We show that our DistDepth trained on simulation data only has on-par performance with those trained on real data.

Our DistDepth is especially capable of 1. *attaining zero-shot cross-dataset inference*, and 2. *closing the gap between sim-to-real and real-to-real learning*¹, as shown in Fig. 1. Throughout the work we visualize depth maps in their actual *metric* ranges unless marked as relative depth. We summarize our contributions as follows.

1. We propose DistDepth, a framework that distills depth-domain structure knowledge into a self-supervised depth estimator to obtain highly structured and metric-accurate depth maps.

2. We present SimSIN, a large-scale indoor simulation dataset that fuels the study of self-supervised indoor depth estimation, and a real dataset, UniSIN, that targets at studying the gap between training on simulation and real data.

3. We attain a practical indoor depth estimator: learning without curated depth groundtruth, efficient and effective data collection by simulation, high generalizability, and accurate and real-time inference for depth sensing.

2. Related Work

2.1. Monocular Scene Depth Estimation

Monocular depth estimation has attracted much research interest using learning-based methods to learn a mapping function from image to depth domain: $\mathcal{I} \rightarrow \mathcal{D}$. Categories of the methods include supervised and self-supervised learning paradigms.

2.1.1 Supervised Methods

Supervised learning requires pixel-level depth annotation. Early methods [18–20, 30, 42, 43, 47, 57, 78, 79] perform pixel-level regression of depth values using convolutional neural networks to minimize a loss between predictions and groundtruth. Recently, Bhat *et al.* [4] adopt adaptive bins for depth regression and use vision transformers [17, 48, 71, 80]. MiDaS [59] smartly mixes several datasets to attain large-scale depth training using scale-and-shift-invariant losses. BoostingDepth [52] fuses multi-scale depth cues in MiDaS based on observations from [31], but it takes minutes to post-process a depth map from MiDaS.

¹*a-to-b*: transferring knowledge learned from *a*-domain to *b*-domain

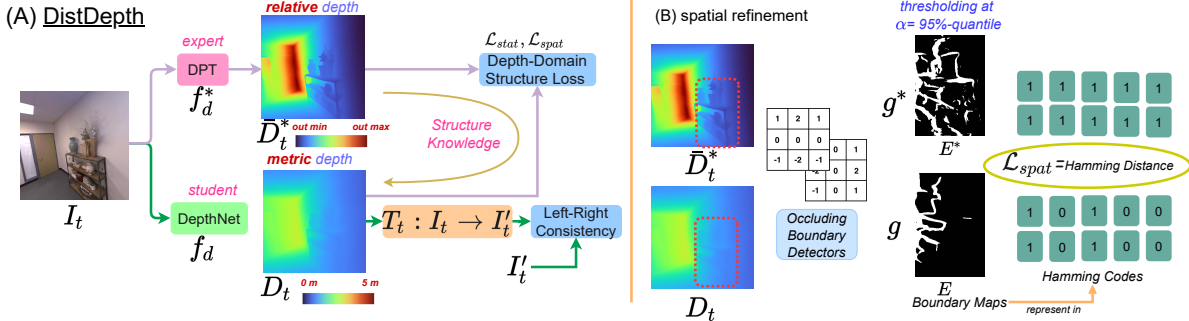


Figure 2. **DistDepth overview.** We distill structures from a pretrained expert network to a student self-supervised depth estimation branch, DepthNet. Such an approach enables us to obtain metric depth maps with fine structures and still work without curated depth annotations. Note that we omit the temporal warping and PoseNet here for simplicity.

DPT (MiDaS-V3) [58] designs a vision transformer and achieves better results than the original MiDaS.

Although state-of-the-art MiDaS [59] and DPT [58] can estimate fine-grained depth structures for *in-the-wild* images, they only provide relative depth, which is up to unknown scale and shift factors to align with actual size due to the mixed-dataset training strategy. These models provide depth for applications like 3D photos where relative depth could be sufficient, but they require finetuning on the target dataset to learn actual ranges. Our DistDepth adopts such pretraining on *in-the-wild* scenes as an expert for depth structure distillation in order to attain both structured and metric-accurate depth from self-supervised learning for indoor domain-focused range sensing.

2.1.2 Self-Supervised Methods

Recent research interest attends to self-supervised methods to lift requirements on groundtruth depth for training, which steps closer to practical depth sensing [26, 38, 40, 41, 54]. MonoDepth [24] learns depth from stereo pairs and utilizes the left-right consistency with photometric loss minimization. MonoDepth2 [25] further includes temporal neighboring frames and also minimizes photometric consistency losses. DepthHints [75] adopts pre-computed SGM [28, 29] depth from stereo pairs as a proxy and still stay self-supervised. ManyDepth [76] uses test-time multi-frame inputs with cost-volume minimization to obtain more accurate predictions. However, these methods all focus on driving scenarios, and their applicability to indoor data is yet to be investigated. Our work is based on self-supervised learning of left-right and temporal consistency with depth structure distillation to attain highly structured and metric-accurate depth for the indoor domain. Some other works attain self-supervision by only temporal consistency [5, 33] without left-right consistency, which makes scale less robust and also needs finetuning on target datasets. Another work [44], based on Manhattan world assumption, minimizes co-planar and normal losses. They only show robustness to planar regions and its scale is inherently ambiguous.

3. Method

3.1. Basic Problem Setup

We describe the commonly adopted left-right and temporal photometric consistency in self-supervised methods such as MonoDepth2, DepthHints, and ManyDepth in this section. During training, I_t and I'_t are stereo pairs at timestep t . DepthNet f_d is used to predict depth of I_t , $D_t = f_d(I_t)$. With known camera intrinsic parameters K and transformation $T_t : I_t \rightarrow I'_t$ using stereo baseline, one can back-project I_t into 3D space and then re-project to the imaging plane of I'_t by utilizing K , D_t , and T_t . $\hat{I}'_t = I_t \langle \text{proj}(D_t, T_t, K) \rangle$ denotes the reprojection. Then the objective is to minimize photometric loss $\mathcal{L} = pe(I'_t, \hat{I}'_t)$, where pe is formulated as follows.

$$pe(I'_t, \hat{I}'_t) = \kappa \frac{1 - \text{SSIM}(I'_t, \hat{I}'_t)}{2} + (1 - \kappa) L_1(I'_t, \hat{I}'_t), \quad (1)$$

where κ is commonly set to 0.85, SSIM [73] is used to measure the image-domain structure similarity, L_1 is used to compute the pixel-wise difference. $pe(I'_t, \hat{I}'_t)$ measures photometric reconstruction error of a stereo pair to attain left-right consistency.

Temporal neighboring frames are also utilized to compute photometric consistency. PoseNet calculates relative camera pose between timestep t and $t + k$: $T_{t+k \rightarrow t} = f_p(I_t, I_{t+k})$ with $k \in \{1, -1\}$. Then, temporal consistency is attained by warping an image from $t + k$ to t and calculating photometric consistency in Eq. 1. At inference time, depth is predicted from a monocular image via $D = f_d(I)$.

Applicability We train MonoDepth2, DepthHints, and ManyDepth on the SimSIN dataset and exemplify the scene fitting later in Fig. 4. Prior arts fit the training set but do not generalize well for cross-dataset evaluation due to complex object arrangements, textures, and patterns for indoor environments.

3.2. DistDepth: Structure Distillation from Expert

To overcome the generalizability issue when applying self-supervised frameworks to indoor environments, we

propose DistDepth (Fig. 2). DPT is adopted as the expert network, which produces highly structured but only relative depth values by $D_t^* = f_d^*(I_t)$ ² as explained in Sec. 2.1.1. We distill the depth-domain structure of D_t^* to the student of self-supervised depth estimation framework, including DepthNet f_d and PoseNet f_p . The self-supervised framework learns metric depth since it leverages stereo pairs with known camera intrinsic and baseline with depth warping operation $I_t \langle \text{proj}(D_t, T_t, K) \rangle$. Such an approach enables f_d to produce both highly structured and metric depth and still work in a self-supervised fashion without groundtruth depth for training.

We first estimate rough alignment factors of scale a_s and shift a_t from DPT’s output D_t^* to predicted depth D_t by minimizing differences between $\bar{D}_t^* = a_s D_t^* + a_t$ and D_t with closed-form expressions from the least-square optimization (see the supplementary).

Statistical loss. Compared with image-domain structure, depth-domain structures exclude depth-irrelevant low-level cues such as textures and painted patterns on objects and show geometric structures. Image-domain structure similarity can be obtained by SSIM [72–74] from a statistical perspective. Depth-domain structure also correlates to its depth value distribution represented by mean, variance, and co-variance for similarity measures. Thus, we compute the SSIM with depth map input \bar{D}_t^* and D_t , and use the negative metric as the loss term

$$\mathcal{L}_{\text{stat}} = 1 - \text{SSIM}(\bar{D}_t^*, D_t), \quad (2)$$

Unlike the widely-used appearance loss that combines SSIM with L_1 loss, we find that pixel-wise difference measures lead to unstable training since inverting from disparity to depth magnifies prediction uncertainty and produces much larger outliers.

Spatial refinement loss. Structure similarity loss only controls the statistically predicted depth distribution and loses spatial information. We next propose a spatial control using occluding boundary map consistency. The Sobel filter, which is a first-order gradient operator [34], is applied to compute depth-domain gradients: $g = (\frac{\partial X}{\partial u}, \frac{\partial X}{\partial v})$, where $X \in \{\bar{D}_t^*, D_t\}$ and u, v represent horizontal and vertical direction on 2D grids. Then we calculate a turn-on level $\alpha = \text{quantile}(\|g\|_2, 95\%)$ at the 95%-quantile level of gradient maps to determine the depth occluding boundaries, where gradients are larger than α . We compute the 0/1 binary-value maps, E^* and E , to represent occluding boundary locations by thresholding \bar{D}_t^* and D_t with their respective α s. Last we calculate the Hamming distance, i.e. bitwise difference, of E^* and E and normalize it by the map

²DPT (and MiDaS) outputs relative relation in disparity (inverse depth) space since it trains on diverse data sources (laser-based depth, depth from SfM, or stereo with unknown calibration). We inverse its outputs and compute losses in the depth space since our training data source is single

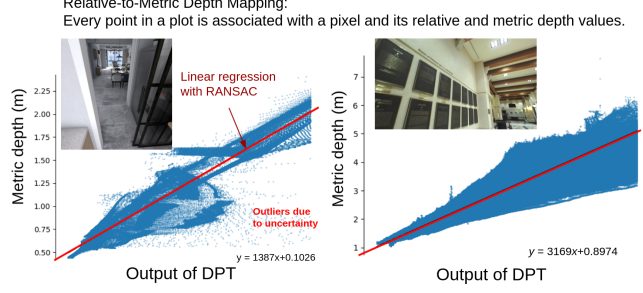


Figure 3. Mapping from relative depth to metric depth is non-trivial. x -axis captures (inverse) output values of DPT and y -axis represents metric depth from simulation systems or sensors. We run least-square linear regression with RANSAC to produce the optimal fitted lines between relative depth and metric depth for random scenes from our dataset.

size and use it as the spatial loss term,

$$\mathcal{L}_{\text{spat}} = E^* \oplus E / |E|, \quad (3)$$

where \oplus is the XOR operation for two boolean sets, and $|E|$ computes the cardinality (size) of the set. In implementation, to make thresholding and binarization operations differentiable, we subtract respective α s from \bar{D}_t^* and D_t and apply soft-sign function, which resembles the sign function but back-propagates smooth and non-zero gradients, to obtain maps with values in $\{-1, 1\}$. After the division by 2, we arrive at the element-wise Hamming distance between the maps. The loss function for structure distillation is $\mathcal{L}_{\text{dist}} = \mathcal{L}_{\text{stat}} + 10^{-1} \mathcal{L}_{\text{spat}}$. The final loss function \mathcal{L}_t for I_t is combined with left-right consistency $\mathcal{L}_{\text{LR}} = \text{pe}(I'_t, \hat{I}_t)$, temporal consistency $\mathcal{L}_{\text{temp}} = \text{pe}(I_t, \hat{I}_{t+k \rightarrow t})$, where $\hat{I}_{t+k \rightarrow t}$ is forward warping and backward warping, $k \in \{1, -1\}$, and $\mathcal{L}_{\text{dist}}$:

$$\mathcal{L}_t = \mathcal{L}_{\text{LR}} + \mathcal{L}_{\text{temp}} + 10^{-1} \mathcal{L}_{\text{dist}}. \quad (4)$$

Compared with self-supervised frameworks, the structure distillation branch gears up the student depth estimator with higher generalizability to unseen textures that better separate depth-relevant and depth-irrelevant low-level cues. On the reverse perspective, the student self-supervised framework helps DPT learn indoor ranges across different indoor scenes. Note that one other intuitive way is to predict scale and shift factors based on DPT to align with metrics. This seemly simple method, however, suffers from the disadvantage that depth estimation from neural networks inevitably includes uncertainty, which is either caused by neural network model or caused by data [35, 36, 50]. Thus, conversion between relative depth and metric depth shows overall linear but noisy trends, and the optimal line equations can vary a lot for different scenes, as shown in Fig. 3.

We adopt ResNet [27] as the backbone for f_d . Although one can use a dense vision transformer for higher prediction accuracy or simply use pretrained DPT f_d^* to replace the DepthNet f_d , they suffer from low inference speed for real-time on-device depth sensing due to larger network size

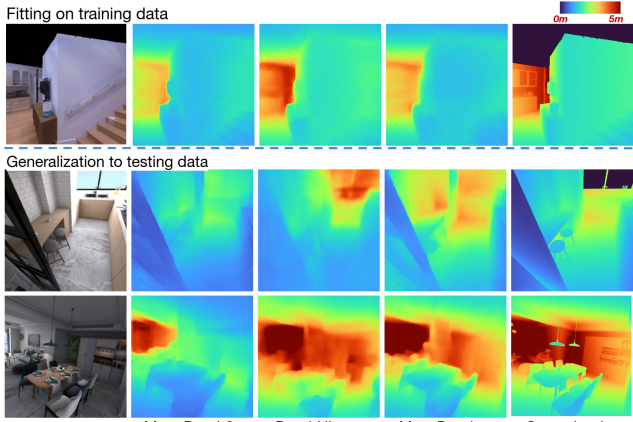


Figure 4. **Intra-/ Inter-Dataset inference.** Prior self-supervised works can fit training data (SimSIN) as shown in the first row, but they do not generalize well when inferring on other datasets such as VA, shown in the second and third rows.

and complex operations. Therefore, we maximally exploit structure knowledge embedded in DPT and also downsize the large vision transformer to smaller-size ResNet, which enables us to run depth sensing at an interactive rate (35+ fps v.s. 8-11 fps for different version DPT, measured on a laptop with RTX 2080 GPU) to fulfill the practical depth estimator purpose. See the supplementary for demonstration. By contrast, BoostingDepth [52] still needs MiDaS or DPT at the inference stage and takes huge processing time for high-resolution depth.

4. Datasets

4.1. Training: SimSIN

To utilize the left-right and temporal neighboring frames to attain photometric consistency for self-supervised training, we adopt the popular Habitat simulator [61, 69] that initiates a virtual agent and renders camera-captured 3D indoor environments onto images. Much recent work in embodied AI adopts Replica, MP3D, and HM3D as the backend 3D models [10–12, 15, 22, 55].

We collect stereo sequences using a baseline of 13cm which follows the camera setting in [7] for indoor captures and render at 512×512 resolution. We perform the agent navigation multiple times and manually filter out failure images, such as when the agent gets too close to walls or navigates to null spaces. Our dataset consists about 85K, 210K, and 220K images from Replica, MP3D, and HM3D respectively, amounting to a total of 515K stereo images from ~ 1000 various environments in our proposed SimSIN dataset, which is by far the largest stereo dataset for generic indoor environments.

4.2. Training: UniSIN

To investigate the gap between simulation and reality and compare performances of models trained on simula-

tion and trained on real data. We utilize ZED-2i [3], a high-performing stereo camera system, to collect large-scale stereo sequences from various interior spaces around a university and create the UniSIN dataset. Its training split contains 500 sequences, and each sequence has 200 stereo pairs, amounting to 200K training images.

4.3. Evaluation Sets

Commercial-Quality simulation. We first select a delicately designed virtual apartment (VA) and render about 3.5K photorealistic images along a trajectory as the evaluation set [1, 2]. The VA dataset contains challenging indoor scenes for depth sensing, such as cabinet cubes with different lighting, thin structures, and complex decorators. These scenes enable us to conduct a detailed study of depth sensing in private indoor spaces, the most common use cases for AR/VR. We further include samples from pre-rendered *Hypersim* [60] dataset, which contains monocular images of virtual environments, for qualitative demonstration.

Real Data. We adopt popular NYUv2 [67] whose test set contains 654 monocular images with depth maps from time-of-flight laser using Kinect v1. To compensate for Kinect’s older imaging system and low resolution and serve more practical AR/VR use, we collect 1K high-definition images with finely optimized depth delivered by ZED-2i for numerical evaluation.

We include a sample collection for these datasets in the supplementary.

5. Experiments and Analysis

We set input size to 256×256 , batch size to 24, and epoch number to 10. Adam [37] is used as the optimizer with an initial learning rate of 2×10^{-4} that drops by a factor of 10 at epoch 8 and 10. We adopt common data augmentation of color jittering and random flipping. We use ResNet50 for our PoseNet f_p and ResNet152 for DepthNet f_d , and the same for MonoDepth2, DepthHints, and ManyDepth for comparison in this section.

5.1. Experiments on Simulation Data

We use SimSIN as the training dataset in Sec. 5.1 and evaluate on various commercial-quality simulation data.

Prior self-supervised methods trained on SimSIN. We first directly train MonoDepth2, DepthHints, and ManyDepth on SimSIN following their settings and show fitting on the training data and inference on VA in Fig. 4 to investigate the generalizability. ManyDepth and DepthHints attain better results than MonoDepth2. Geared with structure knowledge from DPT, our DistDepth produces highly regularized depth-domain structures with increased robustness to unseen examples. Our metric estimation also improves, which we believe is due to better structure reasoning and oc-

Table 1. **Quantitative comparison of self-supervised methods on the VA dataset.** Our DistDepth attains much lower errors than prior works for self-supervised depth estimation. DistDepth-M further uses the test-time multi-frame strategy in ManyDepth. See the main text.

Method	Test-Time Single-Frame				Test-Time Multi-Frame		
	MonoDepth2 [25]	DepthHints [75]	DistDepth	Improvement	ManyDepth [76]	DistDepth-M	Improvement
MAE	0.295	0.291	0.253	-14.2%	0.275	0.239	-13.1%
AbsRel	0.203	0.197	0.175	-13.8%	0.189	0.166	-12.2%
RMSE	0.432	0.427	0.374	-13.4%	0.408	0.357	-12.5%
RMSE _{log}	0.251	0.248	0.213	-15.1%	0.241	0.210	-12.9%

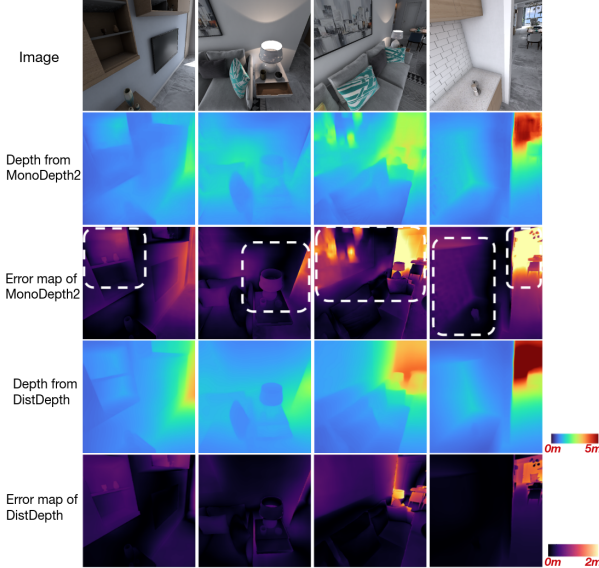


Figure 5. **Qualitative results on VA sequence.** Depth and error maps are shown for DistDepth and MonoDepth2 for comparison. These examples demonstrate that our DistDepth predicts geometrically structured depth for common indoor objects.

cluding boundaries positioning, which together contribute to more accurate range predictions.

Error analysis on VA. The VA dataset includes various challenging scenes in indoor spaces. We show qualitative error analysis in Fig. 5. Highlighted in error maps, our DistDepth has better generalizability on estimating the underlying geometric structures such as paintings, shelves, and walls under various lighting conditions. See supplementary for more examples.

We further show numerical comparison on the entire VA sequence with prior works for self-supervised monocular depth in Table 1. All the methods in comparison are trained on SimSIN. We further equip DistDepth with the test-time multi-frame strategy with cost-volume minimization introduced in ManyDepth and denote this variant by DistDepth-M. Methods are categorized into test-time single-frame and test-time multi-frame. In both cases, DistDepth attains lower errors than prior arts. This validates our network design: with an expert used for depth-domain structure distillation, a student network f_d can produce both structured and metric depth that is closer to the groundtruth.

Ablation study on VA. We first study the expert network

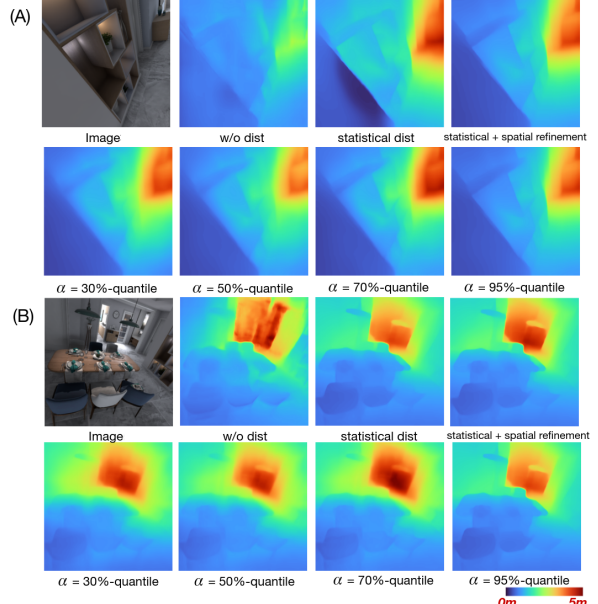


Figure 6. **Qualitative study for depth-domain structure improvement.** Two examples (A) and (B) are shown to study the effects of distillation (dist) losses and turn-on level α in spatial refinement to validate our design in Sec. 3.2.

and adopt different versions of DPT (hybrid and legacy), whose network sizes are different. Table 2 shows that the student network taught by the larger-size expert, DPT-legacy, achieves lower depth estimation errors. Without distillation, results are worse because its estimation relies only on the photometric loss, which fails on untextured areas like walls. As a sanity check, we also provide results of supervised training using SimSIN’s groundtruth depth with pixel-wise MSE loss and test on the VA dataset, which shows the gap between training on curated depth and depth from expert network’s predictions.

We next study the training strategy with different distillation losses and effects of turn-on level α in Sec. 3.2. We compare (1) w/o distillation, (2) distillation with statistical loss only, and (3) distillation with statistical and spatial refinement loss. We demonstrate qualitative results in Fig. 6 to show the depth-domain structure improvements. Without distillation (dist), spatial structures cannot be reasoned crisply. With statistical refinement, depth structures are more distinct. With further spatial refinement, the depth-domain structures show fine-grained details. We further an-

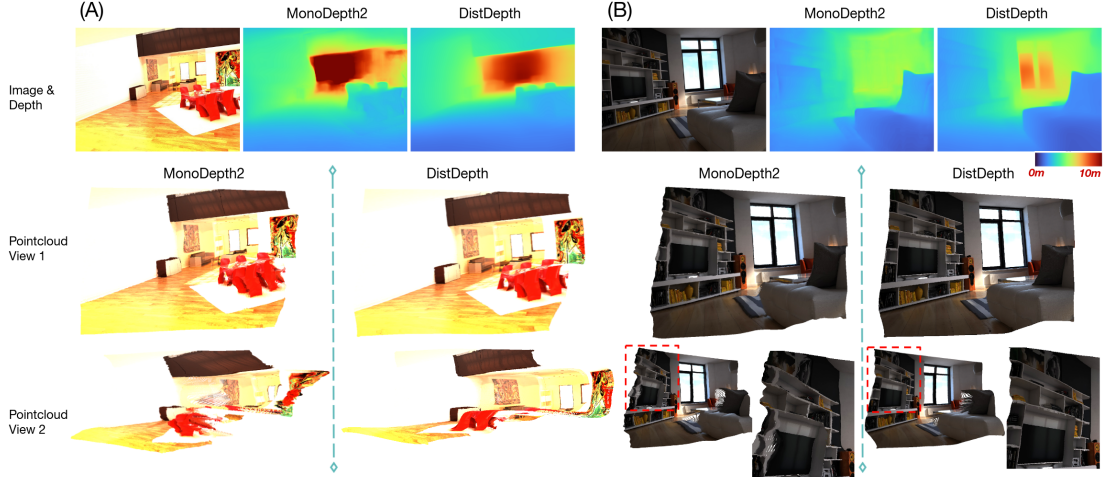


Figure 7. **Results on Hypersim.** Depth map and textured pointcloud comparison of MonoDepth2 and our DistDepth. With structure distillation, DistDepth attains better object structure predictions, such as tables and paintings on the wall shown in (A) and much less distortion for the large bookcase in (B).

Table 2. **Study on the choice of the expert network for distillation.** Different versions of DPT [58] that vary in network sizes (# of params) are adopted as the expert to teach the student. DPT-legacy localizes occluding contours better and leads to a better-performing student network. The results from supervised training are provided as a reference.

Expert	Self-Supervised			Supervised
	w/o distillation	DPT - hybrid	DPT - legacy	
# of params	-	123M	344M	-
MAE	0.295	0.276	0.253	0.221
AbsRel	0.203	0.188	0.175	0.158
RMSE	0.432	0.394	0.374	0.325
RMSE _{log}	0.251	0.227	0.213	0.188

alyze the effects of different turn-on levels of α . Low α makes the structures blurry since the refinement does not focus on the high-gradient occluding boundaries as high α does, which creates the occluding boundary map on high-gradient areas only, which benefits depth-domain structure preservation.

Comparison on Hypersim. We next exhibit depth and pointcloud with textures in Fig. 7 for some scenes in Hypersim. Two different views are adopted for pointcloud visualization. One can find that our DistDepth predicts better geometric shapes of objects in both depth map and pointcloud. See the supplementary for more examples.

5.2. Experiments on Real Data

Closing sim-to-real gap. We compare results of training on simulation (SimSIN)³ and real data (UniSIN) to investigate the performance gap. We examine (1) training MonoDepth2 [25] on simulation and evaluate on real data, (2) training MonoDepth2 [25] on real data and evaluate on real data, (3) training DistDepth on simulation and evaluate

³To balance the training dataset size, we randomly subsample about 200K images here in SimSIN to match UniSIN’s dataset size.

on real data, and (4) training DistDepth on real and evaluate on real data. Fig. 8 illustrates the results of the four settings. Comparing (1) and (2), one can find that MonoDepth2 trained on real data produces more reliable results than on simulation. By contrast, this gap becomes unobvious when comparing settings (3) and (4) using DistDepth. Results of (3) are on-par with (4) and sometimes even produce better geometric shapes like highlighted areas. We further include numerical analysis in the supplementary.

The results validate our proposals on both method and dataset levels. First, DistDepth utilizes an expert network to distill knacks of structures to the student. The distillation substantially adds robustness to models trained on simulation data and makes the results comparable to models trained on real data. This shows the ability of DistDepth for *closing the gap between simulation and real data*. Second, stereo simulation data provide a platform for self-supervised left-right consistency to learn metric depth from stereo triangulation. We show a collection of results in Fig. 9 using DistDepth that is trained purely on simulation.

Evaluation on NYUv2. Table 3 shows evaluations on NYUv2. We first train our DistDepth on SimSIN and finetune on NYUv2 with only temporal consistency. Note that one finetuned model (Sup: Δ) is categorized as semi-supervised since it utilizes an expert that has been trained with NYUv2’s curated depth. The finetuned models produce the best results among the self-supervised methods and even attain comparable results to many supervised methods. We next train DistDepth only on simulation (SimSIN) or real data (UniSIN) and evaluate on NYUv2. Performances of the model trained on SimSIN only drop a little compared with that trained on UniSIN, which justifies our sim-to-real advantage again. Without involving any training data in NYUv2, DistDepth still achieves comparable performances to many supervised and self-supervised methods, which fur-

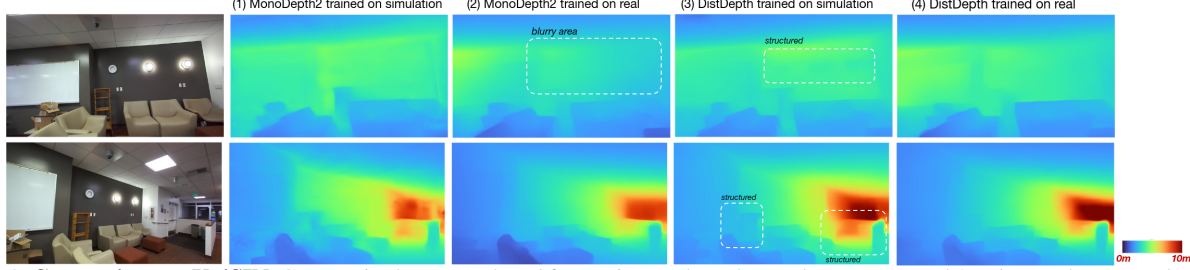


Figure 8. **Comparison on UniSIN.** Geometric shapes produced from DistDepth are better than MonoDepth2. DistDepth concretely reduces the gap for sim-to-real: (3) and (4) attains on-par results and sometimes training on simulation shows better structure than training on real.

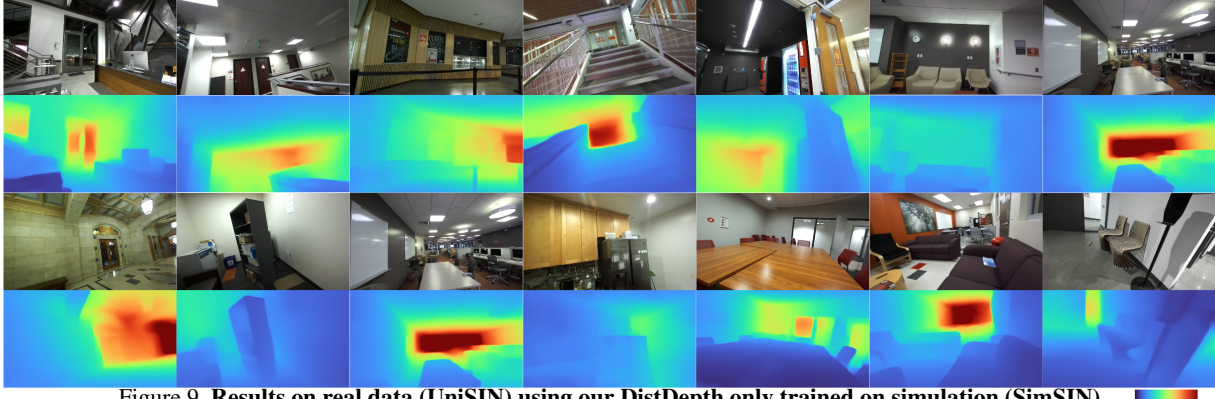


Figure 9. **Results on real data (UniSIN) using our DistDepth only trained on simulation (SimSIN).**

Table 3. **Evaluation on NYUv2.** Sup: ✓ - supervised learning using groundtruth depth, ✗ - not using groundtruth depth, and △ - semi-supervised learning (we use the expert finetuned on NYUv2, where we have indirect access to the groundtruth). We achieve the best results among all self-supervised methods, and our semi-supervised and self-supervised finetuned on NYUv2 even outperform many supervised methods. The last two rows show results without groundtruth supervision and without training on NYUv2. In this challenging *zero-shot cross-dataset evaluation*, we still achieve comparable performances to many methods trained on NYUv2. Error and accuracy (yellow/green) metrics are reported.

Methods	Sup	Train on NYUv2	AbsRel	RMSE	δ_1	δ_2	δ_3
Make3D [62]	✓	✓	0.349	1.214	44.7	74.5	89.7
Li <i>et al.</i> [45]	✓	✓	0.143	0.635	78.8	95.8	99.1
Eigen <i>et al.</i> [18]	✓	✓	0.158	0.641	76.9	95.0	98.8
Laina <i>et al.</i> [42]	✓	✓	0.127	0.573	81.1	95.3	98.8
DORN [20]	✓	✓	0.115	0.509	82.8	86.5	99.2
AdaBins [4]	✓	✓	0.103	0.364	90.3	98.4	99.7
DPT [58]	✓	✓	0.110	0.357	90.4	98.8	99.8
Zhou <i>et al.</i> [82]	✗	✓	0.208	0.712	67.4	90.0	96.8
Zhao <i>et al.</i> [81]	✗	✓	0.189	0.686	70.1	91.2	97.8
Bian <i>et al.</i> [5]	✗	✓	0.157	0.593	78.0	94.0	98.4
StructDepth [44]	✗	✓	0.142	0.540	81.3	95.4	98.8
MonoIndoor [33]	✗	✓	0.134	0.526	82.3	95.8	98.9
DistDepth (finetuned)	✗	✓	0.130	0.517	83.2	96.3	99.0
DistDepth (finetuned)	△	✓	0.113	0.444	87.3	97.4	99.3
DistDepth (SimSIN)	✗	✗	0.164	0.566	77.9	93.5	98.0
DistDepth (UniSIN)	✗	✗	0.158	0.548	79.1	94.2	98.5

ther validates our *zero-shot cross-dataset advantage*.

Finally, we exhibit real-time depth sensing and downstream applications using our estimated depth, such as 3D photos and depth-aware AR effects, in the supplementary.

6. Conclusion and Discussion

This work targets at a practical indoor depth estimation framework with the following features: self-supervised, effective training on simulation, high generalizability, and accurate and real-time inference. We first identify the challenges of indoor depth estimation and study the applicability of existing self-supervised methods with left-right consistency on SimSIN. Geared up with the depth-domain structure knowledge distilled from an expert, we see substantial improvement in both inferring finer structures and more accurate metric depth. We show zero-shot cross-dataset inference that proves its generalizability to work on heterogeneous data domains and attain a broadly applicable depth estimator for indoor scenes. Even more, depth learned from simulation data transfers well to real scenes, which shows the success of our distillation strategy. At inference time, it only takes a single feed-forward pass to DepthNet to produce structured metric depth and reach 35+ fps on a portable device which serves real-time needs.

Limitations. Although DistDepth is capable of producing structured and metric depth using a single forward pass of depth estimation, it operates on a per-frame basis, which can be refined to produce more temporally consistent depth for video inputs [39, 49]. It is still an open question to design a real-time and highly structured video depth estimator. Another remaining issue common for left-right consistency-based depth estimation models is the proper handling of reflective objects. With distillation, DistDepth can produce

estimation for objects with clear contours, as illustrated in Fig. 1 of bulbs. However, our approach is still not yet robust to large mirrors. A possible solution is to locate the mirrors and perform depth completion [83] on depth estimates.

References

- [1] Unreal engine 4. <https://www.unrealengine.com/en-US/unreal>. 2, 5, 1
- [2] Warm harbor environment. <https://www.unrealengine.com/marketplace/en-US/product/warmharbor>. 2, 5, 1
- [3] Zed2i-stereolabs. <https://www.stereolabs.com/zed-2i/>. 5
- [4] Shariq Farooq Bhat, Ibraheem Alhashim, and Peter Wonka. Adabins: Depth estimation using adaptive bins. In *CVPR*, 2021. 2, 8
- [5] Jia-Wang Bian, Huangying Zhan, Naiyan Wang, Zhichao Li, Le Zhang, Chunhua Shen, Ming-Ming Cheng, and Ian Reid. Unsupervised scale-consistent depth learning from video. *IJCV*, 2021. 3, 8
- [6] D. J. Butler, J. Wulff, G. B. Stanley, and M. J. Black. A naturalistic open source movie for optical flow evaluation. In *ECCV*, 2012. 2, 1
- [7] Rohan Chabra, Julian Straub, Christopher Sweeney, Richard Newcombe, and Henry Fuchs. Stereodrnet: Dilated residual stereonet. In *CVPR*, 2019. 5
- [8] Angel Chang, Angela Dai, Thomas Funkhouser, Maciej Halber, Matthias Niebner, Manolis Savva, Shuran Song, Andy Zeng, and Yinda Zhang. Matterport3D: Learning from RGB-D data in indoor environments. In *3DV*, 2017. 2, 1
- [9] Ming-Fang Chang, John W Lambert, Patsorn Sangkloy, Jagjeet Singh, Slawomir Bak, Andrew Hartnett, De Wang, Peter Carr, Simon Lucey, Deva Ramanan, and James Hays. Argoverse: 3D tracking and forecasting with rich maps. In *CVPR*, 2019. 2, 1
- [10] Changan Chen, Ziad Al-Halah, and Kristen Grauman. Semantic audio-visual navigation. In *CVPR*, pages 15516–15525, 2021. 5
- [11] Changan Chen, Unnat Jain, Carl Schissler, Sebastia Vicenc Amengual Gari, Ziad Al-Halah, Vamsi Krishna Ithapu, Philip Robinson, and Kristen Grauman. Soundspace: Audio-visual navigation in 3D environments. In *ECCV*, 2020. 5
- [12] Changan Chen, Sagnik Majumder, Ziad Al-Halah, Ruohan Gao, Santhosh Kumar Ramakrishnan, and Kristen Grauman. Learning to set waypoints for audio-visual navigation. In *ICLR*, 2020. 5
- [13] Sunglok Choi, Taemin Kim, and Wonpil Yu. Performance evaluation of ransac family. *Journal of Computer Vision*, 24(3):271–300, 1997. 2
- [14] Marius Cordts, Mohamed Omran, Sebastian Ramos, Timo Rehfeld, Markus Enzweiler, Rodrigo Benenson, Uwe Franke, Stefan Roth, and Bernt Schiele. The cityscapes dataset for semantic urban scene understanding. In *CVPR*, 2016. 1, 2
- [15] Victoria Dean, Shubham Tulsiani, and Abhinav Gupta. See, hear, explore: Curiosity via audio-visual association. In *NeurIPS*, 2020. 5
- [16] Tom van Dijk and Guido de Croon. How do neural networks see depth in single images? In *ICCV*, 2019. 1
- [17] Alexey Dosovitskiy, Lucas Beyer, Alexander Kolesnikov, Dirk Weissenborn, Xiaohua Zhai, Thomas Unterthiner, Mostafa Dehghani, Matthias Minderer, Georg Heigold, Sylvain Gelly, et al. An image is worth 16x16 words: Transformers for image recognition at scale. In *ICLR*, 2021. 2
- [18] David Eigen and Rob Fergus. Predicting depth, surface normals and semantic labels with a common multi-scale convolutional architecture. In *ICCV*, 2015. 2, 8
- [19] David Eigen, Christian Puhrsch, and Rob Fergus. Depth map prediction from a single image using a multi-scale deep network. *NeurIPS*, 2014. 2
- [20] Huan Fu, Mingming Gong, Chaohui Wang, Kayhan Batmanghelich, and Dacheng Tao. Deep ordinal regression network for monocular depth estimation. In *CVPR*, 2018. 2, 8
- [21] A Gaidon, Q Wang, Y Cabon, and E Vig. Virtual worlds as proxy for multi-object tracking analysis. In *CVPR*, 2016. 2, 1
- [22] Ruohan Gao, Changan Chen, Ziad Al-Halah, Carl Schissler, and Kristen Grauman. Visualechoes: Spatial image representation learning through echolocation. In *ECCV*, 2020. 5
- [23] Andreas Geiger, Philip Lenz, and Raquel Urtasun. Are we ready for autonomous driving? the kitti vision benchmark suite. In *CVPR*, 2012. 1, 2
- [24] Clément Godard, Oisin Mac Aodha, and Gabriel J Brostow. Unsupervised monocular depth estimation with left-right consistency. In *CVPR*, 2017. 1, 3
- [25] Clement Godard, Oisin Mac Aodha, Michael Firman, and Gabriel J. Brostow. Digging into self-supervised monocular depth estimation. In *ICCV*, 2019. 1, 2, 3, 6, 7
- [26] Vitor Guizilini, Rares Ambrus, Sudeep Pillai, Allan Raventos, and Adrien Gaidon. 3D packing for self-supervised monocular depth estimation. In *CVPR*, 2020. 3
- [27] Kaiming He, Xiangyu Zhang, Shaoqing Ren, and Jian Sun. Deep residual learning for image recognition. In *CVPR*, 2016. 4
- [28] Heiko Hirschmuller. Stereo vision in structured environments by consistent semi-global matching. In *CVPR*, 2006. 3
- [29] Heiko Hirschmuller. Stereo processing by semiglobal matching and mutual information. *TPAMI*, 2007. 3
- [30] Junjie Hu, Mete Ozay, Yan Zhang, and Takayuki Okatani. Revisiting single image depth estimation: Toward higher resolution maps with accurate object boundaries. 2019. 2
- [31] Junjie Hu, Yan Zhang, and Takayuki Okatani. Visualization of convolutional neural networks for monocular depth estimation. In *CVPR*, 2019. 2
- [32] Yiwen Hua, Puneet Kohli, Pritish Uplavikar, Anand Ravi, Saravana Gunaseelan, Jason Orozco, and Edward Li. Holopix50k: A large-scale in-the-wild stereo image dataset. In *CVPRW*, 2020. 2, 1

[33] Pan Ji, Runze Li, Bir Bhanu, and Yi Xu. Monoindoor: Towards good practice of self-supervised monocular depth estimation for indoor environments. In *ICCV*, 2021. 3, 8

[34] Nick Kanopoulos, Nagesh Vasanthavada, and Robert L Baker. Design of an image edge detection filter using the sobel operator. *IEEE Journal of solid-state circuits*, 1988. 4

[35] Alex Kendall and Yarin Gal. What uncertainties do we need in bayesian deep learning for computer vision? In *NeurIPS*, 2017. 4

[36] Alex Kendall, Yarin Gal, and Roberto Cipolla. Multi-task learning using uncertainty to weigh losses for scene geometry and semantics. In *CVPR*, 2018. 4

[37] Diederik P Kingma and Jimmy Ba. Adam: A method for stochastic optimization. *arXiv preprint arXiv:1412.6980*, 2014. 5

[38] Marvin Klingner, Jan-Aike Termöhlen, Jonas Mikolajczyk, and Tim Fingscheidt. Self-supervised monocular depth estimation: Solving the dynamic object problem by semantic guidance. In *ECCV*, pages 582–600, 2020. 3

[39] Johannes Kopf, Xuejian Rong, and Jia-Bin Huang. Robust consistent video depth estimation. In *CVPR*, 2021. 8

[40] Varun Ravi Kumar, Marvin Klingner, Senthil Yogamani, Stefan Milz, Tim Fingscheidt, and Patrick Mader. Syndistnet: Self-supervised monocular fisheye camera distance estimation synergized with semantic segmentation for autonomous driving. In *WACV*, 2021. 3

[41] Varun Ravi Kumar, Senthil Yogamani, Markus Bach, Christian Witt, Stefan Milz, and Patrick Mäder. Unrectdepthnet: Self-supervised monocular depth estimation using a generic framework for handling common camera distortion models. In *IROS*, 2020. 3

[42] Iro Laina, Christian Rupprecht, Vasileios Belagiannis, Federico Tombari, and Nassir Navab. Deeper depth prediction with fully convolutional residual networks. In *3DV*, 2016. 2, 8

[43] Jin Han Lee, Myung-Kyu Han, Dong Wook Ko, and Il Hong Suh. From big to small: Multi-scale local planar guidance for monocular depth estimation. *arXiv preprint arXiv:1907.10326*, 2019. 2

[44] Boying Li, Yuan Huang, Zeyu Liu, Danping Zou, and Wenxian Yu. Structdepth: Leveraging the structural regularities for self-supervised indoor depth estimation. In *ICCV*, 2021. 3, 8

[45] Jun Li, Reinhard Klein, and Angela Yao. A two-streamed network for estimating fine-scaled depth maps from single rgb images. In *CVPR*, 2017. 8

[46] Lahav Lipson, Zachary Teed, and Jia Deng. Raft-stereo: Multilevel recurrent field transforms for stereo matching. *3DV*, 2021. 1

[47] Fayaao Liu, Chunhua Shen, and Guosheng Lin. Deep convolutional neural fields for depth estimation from a single image. In *CVPR*, 2015. 2

[48] Ze Liu, Yutong Lin, Yue Cao, Han Hu, Yixuan Wei, Zheng Zhang, Stephen Lin, and Baining Guo. Swin transformer: Hierarchical vision transformer using shifted windows. In *ICCV*, 2021. 2

[49] Xuan Luo, Jia-Bin Huang, Richard Szeliski, Kevin Matzen, and Johannes Kopf. Consistent video depth estimation. *ACM Transactions on Graphics (TOG)*, 2020. 8

[50] Wesley J Maddox, Pavel Izmailov, Timur Garipov, Dmitry P Vetrov, and Andrew Gordon Wilson. A simple baseline for bayesian uncertainty in deep learning. *NeurIPS*, 2019. 4

[51] Nikolaus Mayer, Eddy Ilg, Philip Hausser, Philipp Fischer, Daniel Cremers, Alexey Dosovitskiy, and Thomas Brox. A large dataset to train convolutional networks for disparity, optical flow, and scene flow estimation. In *CVPR*, pages 4040–4048, 2016. 2, 1

[52] S Mahdi H Miangoleh, Sebastian Dille, Long Mai, Sylvain Paris, and Yagiz Aksoy. Boosting monocular depth estimation models to high-resolution via content-adaptive multi-resolution merging. In *CVPR*, 2021. 2, 5

[53] Pushmeet Kohli, Nathan Silberman, Derek Hoiem, and Rob Fergus. Indoor segmentation and support inference from rgbd images. In *ECCV*, 2012. 2

[54] Matteo Poggi, Filippo Aleotti, Fabio Tosi, and Stefano Mattoccia. On the uncertainty of self-supervised monocular depth estimation. In *CVPR*, pages 3227–3237, 2020. 3

[55] Senthil Purushwalkam, Sebastian Vicenc Amengual Gari, Vamsi Krishna Ithapu, Carl Schissler, Philip Robinson, Abhinav Gupta, and Kristen Grauman. Audio-visual floorplan reconstruction. *arXiv preprint arXiv:2012.15470*, 2020. 5

[56] Santhosh K Ramakrishnan, Aaron Gokaslan, Erik Wijmans, Oleksandr Maksymets, Alex Clegg, John Turner, Eric Undersander, Wojciech Galuba, Andrew Westbury, Angel X Chang, et al. Habitat-matterport 3D dataset (HM3D): 1000 large-scale 3D environments for embodied AI. *NeurIPS Datasets and Benchmarks Track*, 2021. 2, 1

[57] Michael Ramamonjisoa and Vincent Lepetit. Sharpnet: Fast and accurate recovery of occluding contours in monocular depth estimation. *ICCVW*, 2019. 2

[58] René Ranftl, Alexey Bochkovskiy, and Vladlen Koltun. Vision transformers for dense prediction. *ICCV*, 2021. 2, 3, 7, 8

[59] René Ranftl, Katrin Lasinger, David Hafner, Konrad Schindler, and Vladlen Koltun. Towards robust monocular depth estimation: Mixing datasets for zero-shot cross-dataset transfer. *TPAMI*, 2020. 2, 3

[60] Mike Roberts and Nathan Paczan. Hypersim: A photorealistic synthetic dataset for holistic indoor scene understanding. *ICCV*, 2021. 2, 5, 1

[61] Manolis Savva, Abhishek Kadian, Oleksandr Maksymets, Yili Zhao, Erik Wijmans, Bhavana Jain, Julian Straub, Jia Liu, Vladlen Koltun, Jitendra Malik, et al. Habitat: A platform for embodied ai research. In *CVPR*, 2019. 2, 5

[62] Ashutosh Saxena, Min Sun, and Andrew Y Ng. Make3D: Learning 3D scene structure from a single still image. *TPAMI*. 8

[63] Daniel Scharstein, Heiko Hirschmüller, York Kitajima, Greg Krathwohl, Nera Nešić, Xi Wang, and Porter Westling. High-resolution stereo datasets with subpixel-accurate ground truth. In *GCPR*, pages 31–42. Springer, 2014. 2, 1

[64] Thomas Schops, Torsten Sattler, and Marc Pollefeys. Bad SLAM: Bundle adjusted direct RGB-D SLAM. In *CVPR*, 2019. 2

[65] Thomas Schöps, Johannes L. Schönberger, Silvano Galliani, Torsten Sattler, Konrad Schindler, Marc Pollefeys, and Andreas Geiger. A multi-view stereo benchmark with high-resolution images and multi-camera videos. In *CVPR*, 2017. 1

[66] Meng-Li Shih, Shih-Yang Su, Johannes Kopf, and Jia-Bin Huang. 3D photography using context-aware layered depth inpainting. In *CVPR*, 2020. 4, 8

[67] Nathan Silberman, Derek Hoiem, Pushmeet Kohli, and Rob Fergus. Indoor segmentation and support inference from rgbd images. In *European conference on computer vision*, 2012. 2, 5, 1

[68] Julian Straub, Thomas Whelan, Lingni Ma, Yufan Chen, Erik Wijmans, Simon Green, Jakob J Engel, Raul Mur-Artal, Carl Ren, Shobhit Verma, et al. The replica dataset: A digital replica of indoor spaces. *arXiv preprint arXiv:1906.05797*, 2019. 2, 1

[69] Andrew Szot, Alex Clegg, Eric Undersander, Erik Wijmans, Yili Zhao, John Turner, Noah Maestre, Mustafa Mukadam, Devendra Chaplot, Oleksandr Maksymets, et al. Habitat 2.0: Training home assistants to rearrange their habitat. *NeurIPS*, 2021. 2, 5, 1

[70] Chaoyang Wang, Simon Lucey, Federico Perazzi, and Oliver Wang. Web stereo video supervision for depth prediction from dynamic scenes. In *3DV*, pages 348–357, 2019. 2, 1

[71] Yulin Wang, Rui Huang, Shiji Song, Zeyi Huang, and Gao Huang. Not all images are worth 16x16 words: Dynamic vision transformers with adaptive sequence length. In *NeurIPS*, 2021. 2

[72] Zhou Wang and Alan C Bovik. A universal image quality index. *Signal Processing Letters*, 2002. 4

[73] Zhou Wang, Alan C Bovik, Hamid R Sheikh, and Eero P Simoncelli. Image quality assessment: from error visibility to structural similarity. *TIP*, 2004. 3, 4

[74] Zhou Wang, Eero P Simoncelli, and Alan C Bovik. Multiscale structural similarity for image quality assessment. In *The Thirti-Seventh Asilomar Conference on Signals, Systems & Computers*, 2003, 2003. 4

[75] Jamie Watson, Michael Firman, Gabriel J Brostow, and Daniyar Turmukhambetov. Self-supervised monocular depth hints. In *ICCV*, 2019. 1, 2, 3, 6

[76] Jamie Watson, Oisin Mac Aodha, Victor Prisacariu, Gabriel Brostow, and Michael Firman. The temporal opportunist: Self-supervised multi-frame monocular depth. In *CVPR*, 2021. 1, 2, 3, 6

[77] Benjamin Wilson, William Qi, Tanmay Agarwal, John Lambert, Jagjeet Singh, Siddhesh Khandelwal, Bowen Pan, Ratnesh Kumar, Andrew Hartnett, Jhony Kaesemeyer Pontes, et al. Argoverse 2.0: Next generation datasets for self-driving perception and forecasting. In *NeurIPS Datasets and Benchmarks Track*, 2021. 2

[78] Dan Xu, Wei Wang, Hao Tang, Hong Liu, Nicu Sebe, and Elisa Ricci. Structured attention guided convolutional neural fields for monocular depth estimation. In *CVPR*, 2018. 2

[79] Wei Yin, Yifan Liu, Chunhua Shen, and Youliang Yan. Enforcing geometric constraints of virtual normal for depth prediction. In *ICCV*, 2019. 2

[80] Li Yuan, Yunpeng Chen, Tao Wang, Weihao Yu, Yujun Shi, Zihang Jiang, Francis EH Tay, Jiashi Feng, and Shuicheng Yan. Tokens-to-token ViT: Training vision transformers from scratch on imagenet. In *ICCV*, 2021. 2

[81] Wang Zhao, Shaohui Liu, Yezhi Shu, and Yong-Jin Liu. Towards better generalization: Joint depth-pose learning without posenet. In *CVPR*, 2020. 8

[82] Junsheng Zhou, Yuwang Wang, Kaihuai Qin, and Wenjun Zeng. Moving indoor: Unsupervised video depth learning in challenging environments. In *CVPR*, 2019. 8

[83] Luyang Zhu, Arsalan Mousavian, Yu Xiang, Hammad Mazhar, Jozef van Eenbergen, Shoubhik Debnath, and Dieter Fox. RGB-D local implicit function for depth completion of transparent objects. In *CVPR*, 2021. 9

Supplemental Materials:

A. Overview

In Sec. B, we provide more details of all datasets and include some samples. We especially focus on our proposed large-scale SimSIN and UniSIN datasets. In Sec. C, we show both numerical and visual analysis on UniSIN’s test set. In Sec. D, we describe the closed-form solutions to the least-square problem used in Sec.3.2 of the paper. In Sec. E, we first create a simple oracle that uses the least-square alignment from DPT’s outputs to groundtruth’s metric depth and evaluate the performance of this oracle method. We then present more studies on our loss combinations. In Sec. F, we explain more on the terms of depth-relevant and depth-irrelevant low-level cues mentioned in paper Sec.3.2. In Sec. G, we present more results on VA and Hypersim. We further present downstream applications using depth maps from our DistDepth, including depth-aware AR effects and 3D photos.

B. Datasets

We show a collection of data samples in Fig. S2 for all datasets we include.

VA and Hypersim: We render a delicately constructed 3D environment [2] using Unreal Engine 4 (UE4) [1], including 7K left-right paired images. This environment contains challenging indoor scenes, such as cabinet cubes with different lighting conditions, thin structures, and complex decorators. We also include several pre-rendered scenes in the Hypersim dataset [60] for qualitative evaluation.

NYUv2: This public dataset [67] includes various indoor scenes captured by Kinect that produces monocular RGB images and depth from the time-of-flight laser system. Although NYUv2 is popular for single-image depth estimation, the images are low-resolution and contain noise due to its older camera model, making it hard to claim practicability in recent AR/VR creation needs. Thus, we also collect our large-scale real dataset for training and evaluation.

SimSIN: This dataset includes 515K left-right paired images using Habitat simulator [69] with 3D environments of Replica [68], MP3D [8], and HM3D [56]. These 3D environments are created by processing real room scans. We use our large-scale SimSIN as the training dataset. One can find that the rendered images from Replica have better quality in both appearance and geometry than MP3D and HM3D, but Replica contains 18 scenes with lower scene variation. In contrast, MP3D and HM3D contain 90 and 900 various scenes. Thus we aggregate these 3D environments to attain higher dataset diversity and also maintain appearance and geometry quality.

UniSIN: The collected UniSIN, including real university scenes using recent high-performing ZED stereo cameras, which contains better imaging quality than NYUv2.

Table S0. Number of sequences for different types of space.

Private room	Office	Hallway	Lounge	Meeting room
45	90	100	100	19
Large room	Classroom	Library	Kitchen	Playroom
33	48	24	29	12

Its training split contains 500 sequences with about 200K left-right images, and the testing data includes 1K images for numerical evaluation. The scenes include private or public spaces, and we organize the number of sequences for each type of space in Table S0.

Both our SimSIN and UniSIN are large-scale datasets of indoor scenes with stereo pairs to fulfill training with left-right consistency. We also enumerate other existing stereo datasets (that are not used in this work) as follows.

(1) Large-scale datasets that focus on driving scenarios: KITTI [23], vKITTI [21], Cityscapes [14], and Argoverse [9].

(2) Indoor datasets but small-scale: Middlebury 2021 (48 images), Middlebury 2014 (66 images) [63], or some scenes in ETH3D two-view Stereo (32 images) [65].

(3) Datasets scraped from web or in-the-wild: WSVD [70] and Holopix50K [32].

(4) Datasets of 3D movies with non-realistic scales: SceneFlow [51] and Sintel [6].

Although category (2) also targets at indoor scenes, they focus on stereo matching algorithms, where smaller numbers of images may be efficient for training [46]. By contrast, our DistDepth is a monocular depth estimation method whose DepthNet only takes a single image and predicts its depth map. Furthermore, the self-supervision fashion inherently requires a larger training dataset since there are no direct mappings from the image-domain to the depth-domain accessible at training time. Therefore, we collect large-scale datasets, SimSIN and UniSIN, to achieve our aims of self-supervised monocular depth estimation with left-right consistency and verify our advantages of closing sim-to-real gaps.

We plot the depth distributions for our newly created datasets, SimSIN and UniSIN, in Fig. S1.

C. Numerical Analysis on UniSIN

We also exhibit numerical analysis on the UniSIN test set that contains 1K images from no-overlapping scenes with the training set in Table S2.

D. Least-Square Alignment

In Sec.3.2 of the paper, we adopt a least-square alignment by minimizing the difference of $a_s D_t^* + a_t$ and D_t , where a_s is the scale term, and a_t is the shift term. For sim-

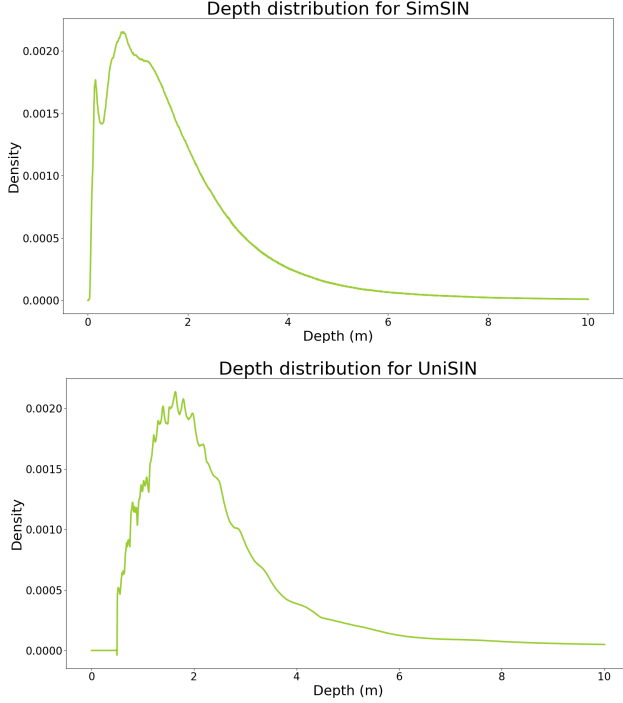


Figure S1. Depth distributions for SimSIN and UniSIN.

Table S2. Numerical analysis on the UniSIN test set. Our DistDepth trained on simulation data can reach similar performances of that trained on real data. Lower errors can be attained compared with MonoDepth2.

Error	MonoDepth2 (Sim)	MonoDepth2 (Real)	DistDepth (Sim)	DistDepth (Real)
MAE	0.610	0.571	0.518	0.505
AbsRel	0.175	0.163	0.135	0.130
RMSE	0.742	0.688	0.623	0.611
RMSE _{log}	0.232	0.200	0.159	0.162

plicity, here we drop time-step notations t in depth terms D_t^* and D_t and use D_i^* to denote indexing depth values at the i -th pixel. Using the above notations, we can write the least-square problem as

$$\min_{a_s, a_t} \sum_i \|a_s D_i^* + a_t - D_i\|^2, \quad (\text{S1})$$

Then, we change symbols with $\vec{d}_i^* = [D_i^*, 1]^\top$ and $\vec{a} = [a_s, a_t]^\top$. Then Eq. S1 becomes

$$\min_{\vec{a}} \sum_i \|\vec{d}_i^{*\top} \vec{a} - D_i\|^2, \quad (\text{S2})$$

which corresponds to the normal form of a least-square problem. Then, the optimal solution of \vec{a} is

$$\vec{a} = \sum_i \left(\vec{d}_i^* \vec{d}_i^{*\top} \right)^{-1} \sum_i \left(\vec{d}_i^* D_i \right). \quad (\text{S3})$$

Table S2. Performances of converting relative depth into metric depth using linear regression. We convert DPT’s outputs to metric depth using linear relations obtained by optimizing the least-square linear regression problem with RANSAC. See the text in Sec. E.

Error	Linear Regression Oracle	MonoDepth2	DistDepth
MAE	0.390	0.295	0.253
AbsRel	0.359	0.203	0.175
RMSE	0.645	0.432	0.374
RMSE _{log}	0.283	0.251	0.213

Table S3. Numerical studies on the DepthNet architecture choices. We adopt ResNet of different numbers of layers as the DepthNet’s architecture and find that deeper ResNet produces lower errors.

Error	ResNet50	ResNet101	ResNet152
MAE	0.261	0.255	0.253
AbsRel	0.182	0.177	0.175
RMSE	0.383	0.377	0.374
RMSE _{log}	0.221	0.217	0.213

E. More Studies

We first present an oracle that converts outputs of large-size DPT pretraining to metric depth using linear relations with groundtruth depth, i.e., using red lines shown in Fig. 3 of the main paper as the converter. We then calculate the depth errors of all points to the regressed line.

Since those regressed lines are optimal in terms of minimizing the least-square errors of inliers using linear regression with RANSAC [13], this oracle is associated with a perfect estimator to predict the slope and intercept for the conversion, and thus its performance can be considered as optimal under the linear relation assumption in DPT [58].

We exhibit the performances in Table S2 on the VA dataset. One can observe that this oracle performs much worse than the MonoDepth2 and DistDepth. The results show that optimal linear mappings are weak in capturing uncertainty in either depth estimation models or data (epistemic or aleatoric uncertainty) that cause outliers in the scatter plots of paper Fig. 3.

We next present numerical ablation studies on the loss term combinations: (1) without distillation: using \mathcal{L}_{LR} and \mathcal{L}_{temp} (2) with distillation of the statistical loss only: using \mathcal{L}_{LR} , \mathcal{L}_{temp} , and \mathcal{L}_{stat} , and (3) full loss terms: using \mathcal{L}_{LR} , \mathcal{L}_{temp} , \mathcal{L}_{stat} , and \mathcal{L}_{spat} . We show the comparison on the VA dataset in Fig. S3.

We further study DepthNet’s architecture using ResNet of different numbers of layers in Table S3, which shows decreasing errors with deeper networks.

Next, we also compare the inference speed in Fig. S4 using commonly used convolutional neural networks (CNN) and Dense Vision Transformer (D-ViT) adopted in DPT.

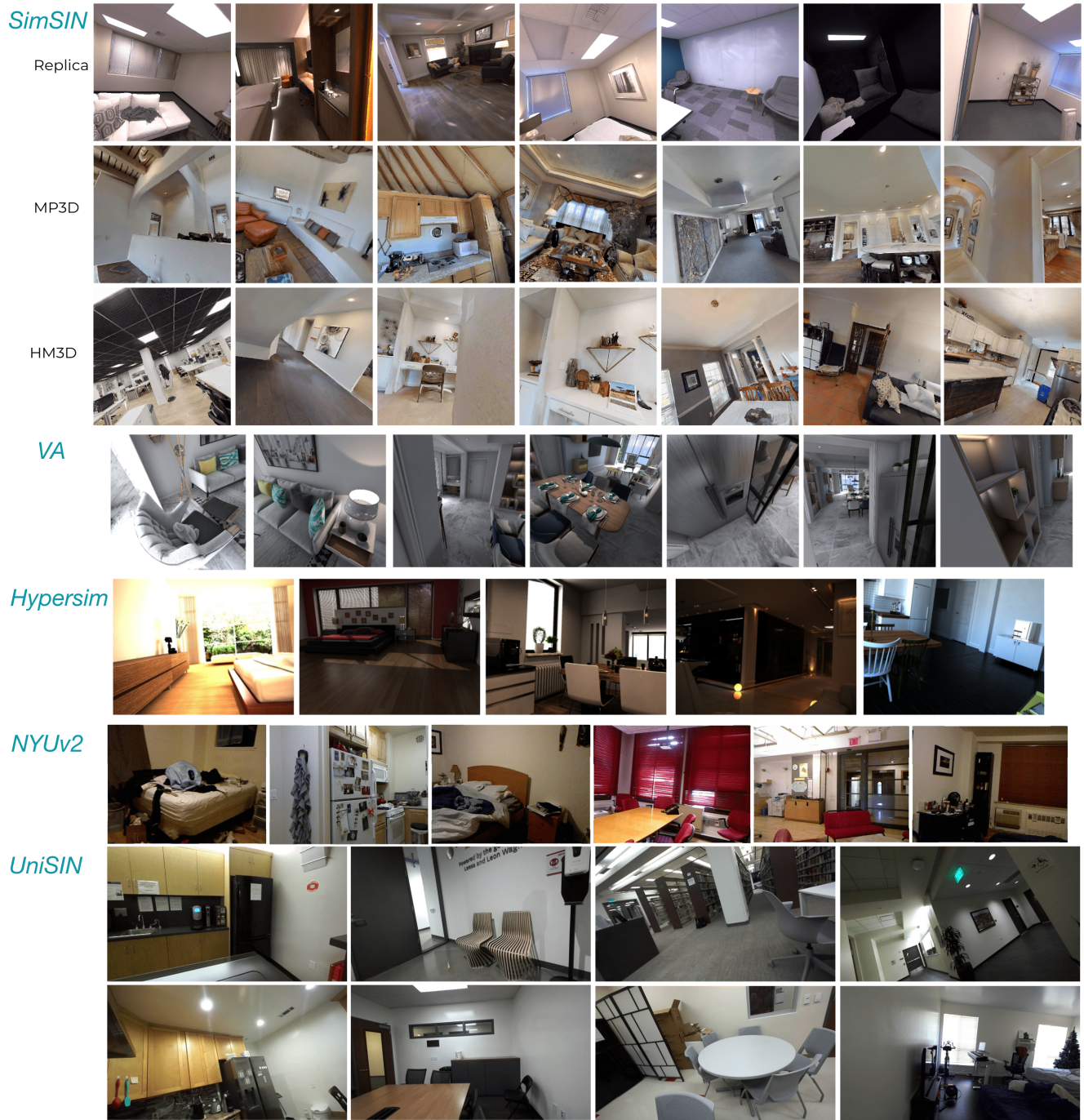


Figure S2. Sample images of all datasets used in this work.

F. Depth-Relevant and Depth-Irrelevant Low-Level Cues

We illustrate how networks “see” depth in Fig. S5. A low-level feature is reasoned as depth-relevant or depth-irrelevant based on its local regions. A well-trained depth estimator can differentiate depth-relevant and depth-

irrelevant features and only produce discontinuous depth values at the depth-relevant positions.

G. More Results

In Fig. S6-S9, we present more comparison with prior self-supervised monocular depth estimation methods, which are all trained on SimSIN. Our DistDepth predicts

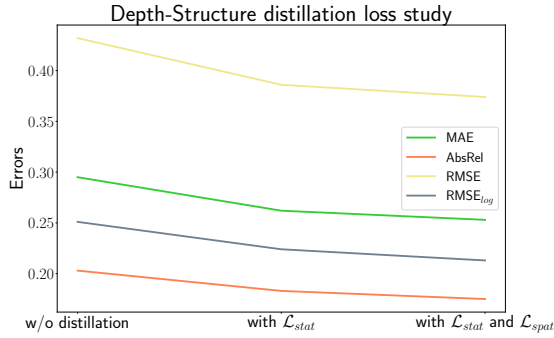


Figure S3. Numerical studies on the loss combination. (1) w/o distillation loss (2) with statistical distillation loss only (3) with full distillation loss.

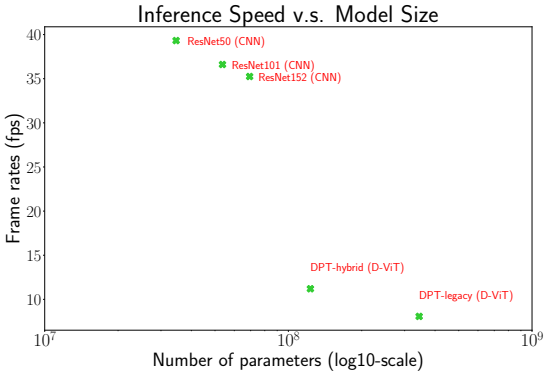


Figure S4. Comparison on inference speed. We test on a portable laptop (with Intel Core i7-10875H CPU and Nvidia RTX 2080 GPU) and compare architectures for DepthNet using convolutional neural network (CNN) and Dense Vision Transformer (D-ViT) introduced in DPT.

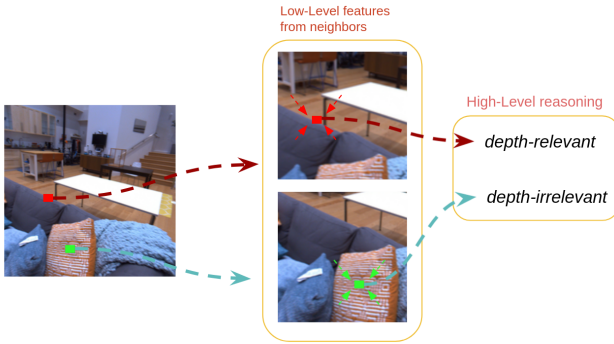


Figure S5. Explanations on depth-relevant and depth-irrelevant low-level cues. Low-Level cues at the red point are depth-relevant since it contains information of depth-domain occluding boundaries to its neighborhood. In contrast, low-level cues at the green point are only textures at the same depth without occluding boundary information. A good depth estimator is capable of separating depth-relevant and depth-irrelevant low-level cues.

better depth maps, lower errors, and also better 3D point cloud than other methods. In addition, we demonstrate downstream applications on 3D photos, using an off-the-

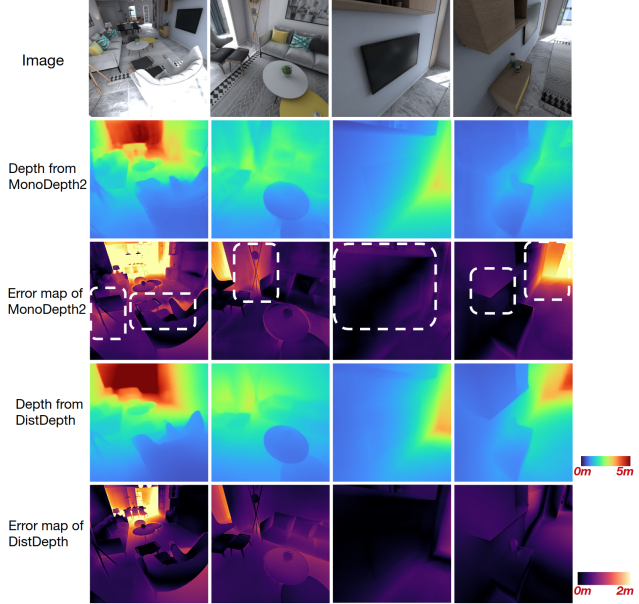


Figure S6. More Results on the VA dataset that extends Fig. 5 of the main paper. Depth and error maps generated by our DistDepth and MonoDepth2 are shown.

shelf 3D photo creation pipeline [66], and depth-aware AR effects in Fig. S10 and S11.

Furthermore, we present several failure cases in Fig. S12.

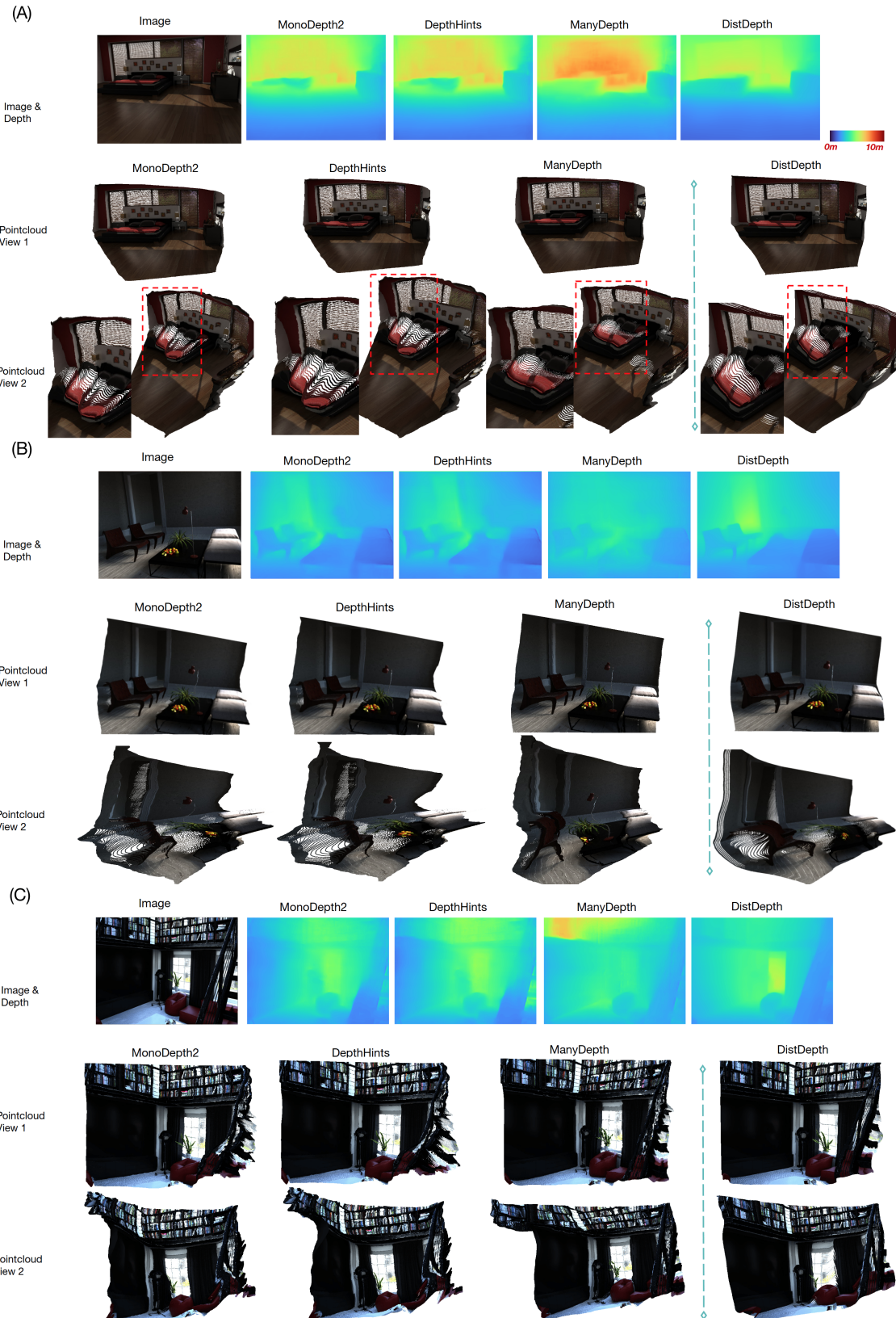


Figure S7. Results on Hypersim. Depth map and textured point cloud comparison of MonoDepth2 and our DistDepth. DistDepth shows less distortion on the edge of the bed in example (A) and more structured walls and chairs in example (B) and (C).

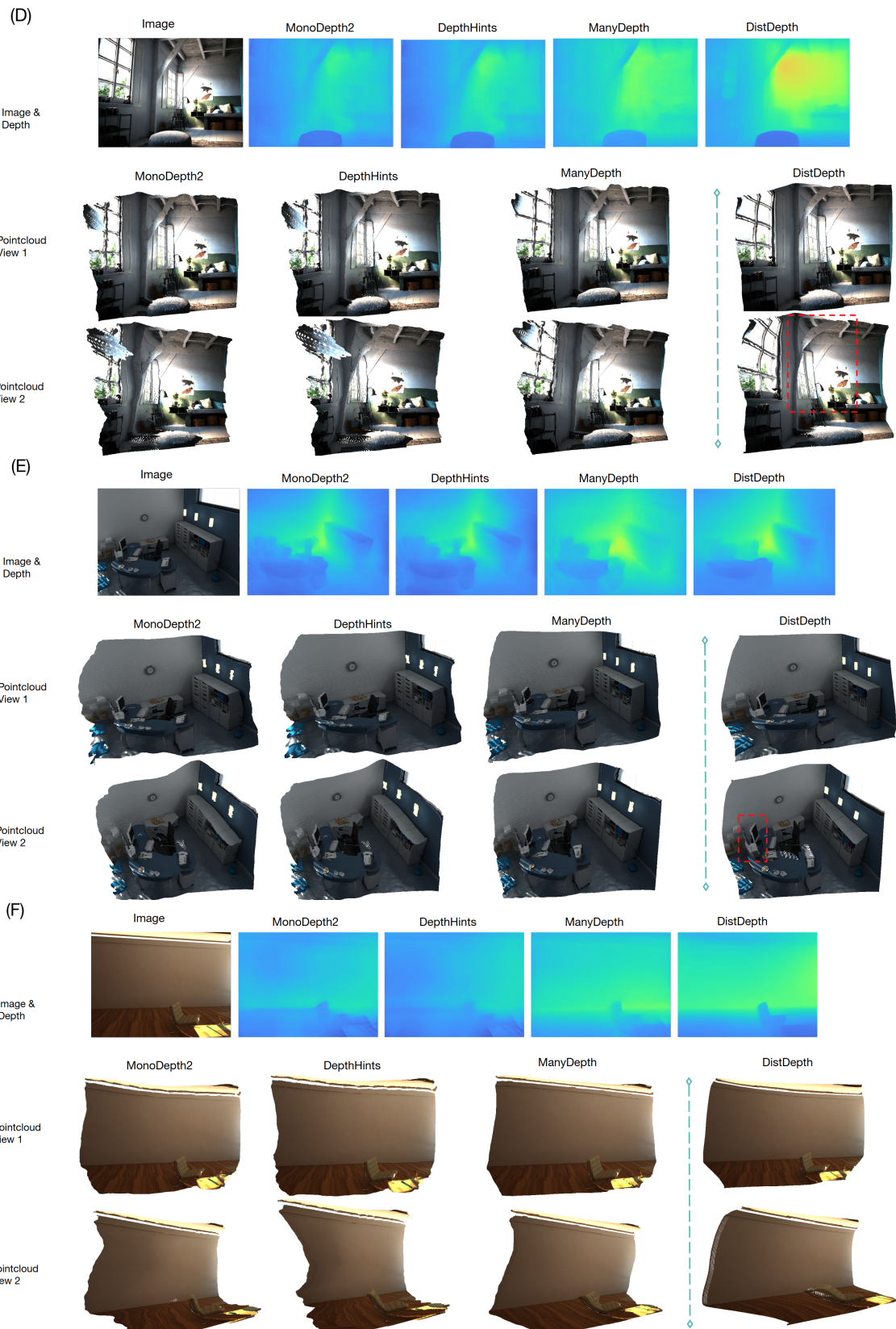


Figure S8. **(Continued) Results on Hypersim.** Our DistDepth's predictions have less distortions of highlighted areas in (D) and (E) and the wall in (F).

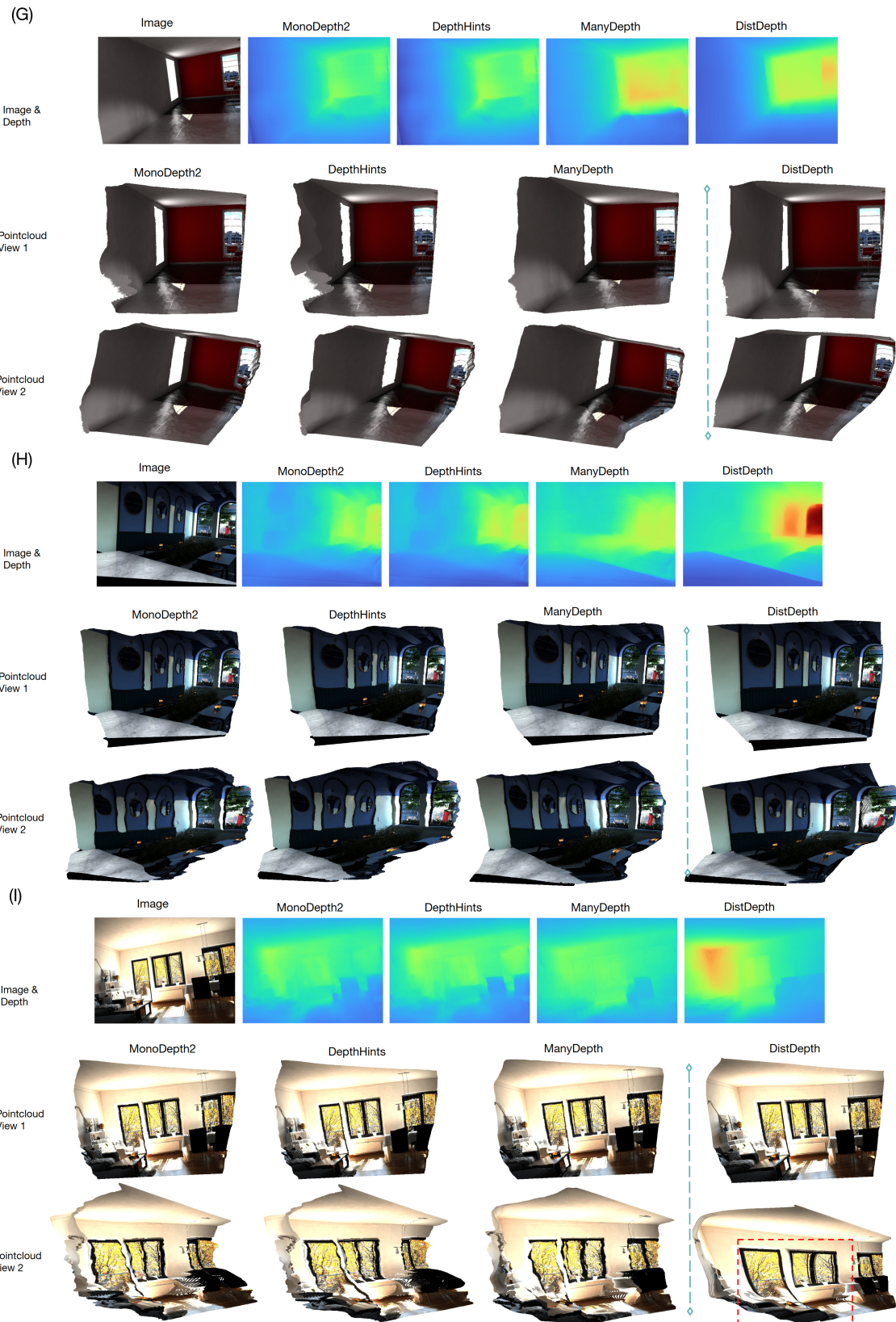


Figure S9. (Continued) Results on Hypersim.

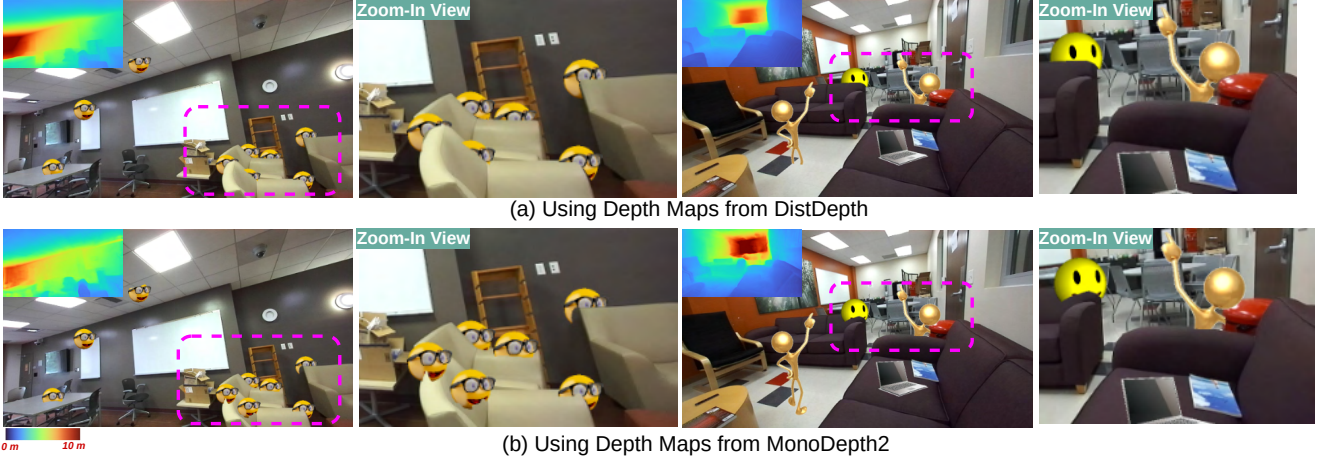


Figure S10. **Exemplar depth-aware AR occlusion effects and comparison.** We insert several virtual objects into scenes with depth maps to maintain *proper occluding boundaries* and interact with objects. Using our DistDepth’s depth maps have more refined and more accurate occluding boundaries.

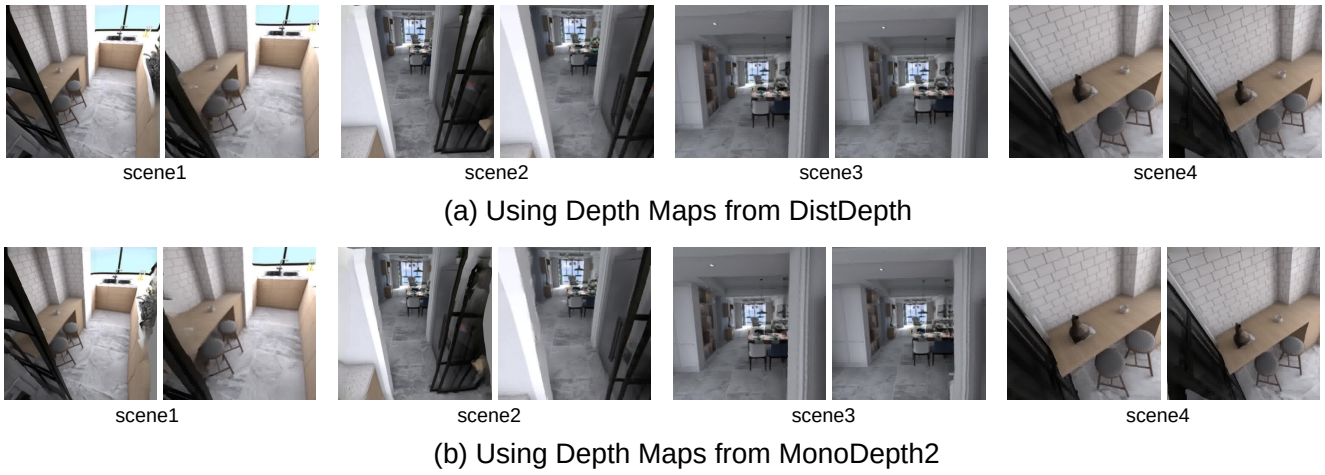


Figure S11. **Exemplar 3D photo creation and comparison.** We use images and the estimated depth maps from our DistDepth and MonoDepth2 as inputs to create 3D photos using an off-the-shelf rendering pipeline [66]. Four scenes and two different views for each scene are exhibited here to exemplify the performances. 3D photos using depth maps from our DistDepth have much less distortions, especially at structures and occluding boundaries.

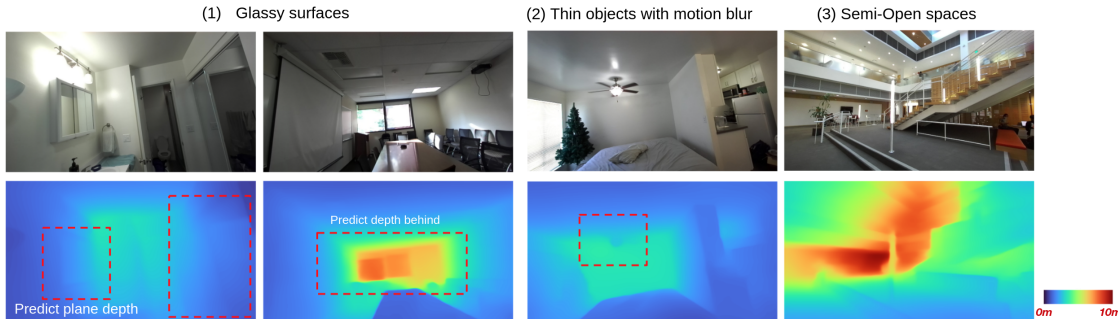


Figure S12. **Failure cases.** (1) Depth values on glossy surfaces may not be perfectly predicted. (2) Structures of thin with motion blur objects may be missing. (3) Training data in either SimSIN or UniSIN are mostly room spaces (see Fig. S1), and we predict metric depth that is robust in the close-range indoor spaces. As a result, predictions in semi-open spaces may be less accurate sometimes.